GPS Solutions (2022) 26:45
https://doi.org/10.1007/s10291-021-01220-0

ORIGINAL ARTICLE

HPL calculation improvement for Chi-squared residual-based ARAIM

Baoyu Liu[1] · Yang Gao[1] · Yuting Gao[1] · Shizhuang Wang[2]

Received: 27 March 2021 / Accepted: 21 December 2021 / Published online: 2 February 2022

Abstract
To obtain the tightest possible horizontal protection level (HPL) for the Chi-squared residual-based advanced receiver autonomous integrity monitoring (ARAIM), it is prerequisite to determine the worst horizontal position error (HPE) distribution center and the worst noncentrality parameter for each fault event hypothesis. By transforming the HPE into a new space, an upper bound for the HPE distribution center is derived which can account for multiple faults, constellation faults and nominal biases. The bound for the noncentrality parameter is given, and an error function-based method is also developed to compute conservative integrity risk which can improve HPL calculation efficiency by avoiding involved integral. A conducted experiment based on GPS (Global Position System), Galileo (European Global Navigation Satellite System) and BDS (BeiDou Navigation Satellite System) ephemeris data show that the proposed algorithm can significantly improve the HPL tightness compared to solution separation-based ARAIM (SS-ARAIM).As per journal instruction, Please provide author's photographies.The author's photos are attached.

Keywords Protection level · Integrity monitoring · ARAIM · Chi-square · Noncentrality parameter

Abbreviations

AL	Alert limits
ARAIM	Advanced receiver autonomous integrity monitoring
BDS	BeiDou navigation satellite system
ENU	East, north, up
GNSS	Global navigation satellite system
GPS	Global position system
HMI	Hazardously misleading information
HPE	Horizontal position error
HPL	Horizontal protection level
ICAO	International Civil Aviation Organization
KF	Kalman filter
MI	Misleading information
PE	Position error
PL	Protection level
RAIM	Receiver autonomous integrity monitoring
SS-ARAIM	Solution separation-based ARAIM
VPE	Vertical position error
VPL	Vertical protection level
WLS	Weighted least squares

Introduction

Integrity is one of the utmost priorities for safety critical GNSS (Global Navigation Satellite System) applications as misleading information (MI) can result in life-threatening problems. With the growing prosperity of autonomous vehicles such as unmanned aerial vehicles and driver-less cars, GNSS integrity attracts increasing attention in aviation applications and beyond. As defined in the GNSS Standards and Recommended Practices by International Civil Aviation Organization (ICAO), integrity is a measure of the trust which can be placed in the correctness of the information supplied by the total system (ICAO 2006). The receiver autonomous integrity monitoring (RAIM) algorithm is one effective approach to address GNSS integrity, which is self-contained and operates on the basis of consistency check on redundant measurements. So far, different kinds of receiver integrity monitoring algorithms have been developed, of which the Chi-squared residual-based RAIM (Parkinson and

✉ Baoyu Liu
baoyu.liu@ucalgary.ca

[1] Department of Geomatics Engineering, University of Calgary, 2500 University Drive NW, Calgary, AB T2N 1N4, Canada

[2] School of Aeronautics and Astronautics, Shanghai Jiao Tong University, 800 Dongchuan Road, Minhang District, Shanghai 200240, China

Axelrad 1988; Sturza 1988) for single-fault scenarios and the solution separation-based RAIM (Brenner 1996; Blanch et al. 2015) for multiple-fault cases are the two most typical ones (Joerger and Pervan 2016).

Integrity monitoring includes the ability to provide timely and valid warnings to users when the navigation solution error exceeds tolerable constraints. The absolute position error (PE) is bounded by protection level (PL) in an integrity monitoring algorithm, and the PL can be divided into vertical protection level (VPL) and horizontal protection level (HPL). Hence, PL calculation is a key part of the design of an integrity monitoring algorithm, and the accuracy of PL calculation is extremely important for effectively monitoring system integrity. The PL is calculated on the basis of the distributions of PE and fault detection statistics and the relationship between them. Although the receiver integrity monitoring performance can be enhanced by various measures such as Kalman filter (KF) (Diesel and Luu 1995; Joerger and Pervan 2013; Bhattacharyya and Gebre-Egziabher 2014, 2015) and the aiding of an inertial navigation system (Tanıl et al. 2018; Wang et al. 2020), the Chi-squared residual-based RAIM and the solution separation-based RAIM are particularly attractive because they have a straightforward set of the theory of such distribution and relationship, as well as the fact that the weighted least squares (WLS) positioning is the GNSS positioning method most extensively used in practice.

Compared to VPL, the HPL is more difficult to calculate because the horizontal position error (HPE) is featured by a two-dimensional normal distribution characterized by covariance and mean (distribution center). Currently, the HPL calculation is generally divided into two components, respectively, accounting for fault bias and measurement noise (Bhattacharyya and Gebre-Egziabher 2014; Brown and Chin 1998; Walter and Enge 1995), or for two orthogonal directions (Blanch et al. 2015). Although such approaches have a great deal of convenience in computation, the relevance between the two components often has not been fully taken into account or made use of, which may lead to an overly conservative HPL (Blanch and Walter 2020a; Jiang and Wang 2016; Milner and Ochieng 2010).

Accurate HPL should be calculated by double integral (Ober 1998). The double integral within the HPL calculation is affected by the HPE distribution center, which indicates the HPE directly caused by GNSS faults and nominal biases, and the HPE distribution center will change when any fault magnitude varies. In the Chi-squared residual-based RAIM, the magnitude of an undetected GNSS fault is represented by the square root of the noncentrality parameter of the noncentral Chi-square distribution of fault detection statistic. Determining the worst noncentrality parameter in each fault event hypothesis that can maximize the probability of MI hence has a significant influence on the accuracy and reliability of HPL (Feng et al. 2006; Jiang and Wang 2014; Milner and Ochieng 2011). A calculated reliable HPL should bound the HPE even in the worst situation which comes with the worst HPE distribution center and the worst noncentrality parameter. The worst noncentrality parameter can be obtained by search method (Blanch and Walter 2020b). Comparatively, finding the worst HPE distribution center is more difficult. Even the worst noncentrality parameter is achieved, determining the worst HPE distribution center in the multi-fault event hypothesis is still challenging as the corresponding trajectory of the HPE distribution center is two dimensional.

We propose an algorithm to calculate the HPL of Chi-squared residual-based ARAIM. In order to bound the HPE distribution center, the HPE is transformed into a new space in which the HPE has a two-dimensional standard normal distribution. The bound of the HPE distribution center caused by multiple faults, constellation faults and nominal biases is derived in the new space. Through constructing an inscribed rectangle of the double integral region in the HPL calculation, an error function-based method for getting conservative integrity risk and corresponding worst noncentrality parameter is also developed. An experiment based on GPS, Galileo and BDS ephemeris data is performed to validate the proposed algorithm, which shows the proposed algorithm can significantly improve the HPL tightness compared to SS-ARAIM.

Chi-squared residual-based RAIM

Integrity requirements can be quantified with three terms: alert limits (AL), time-to-alert and integrity risk. Based on the three terms, an integrity monitoring algorithm can be designed to continuously check system integrity. The GNSS fault is detected according to the continuity risk requirement. If no abnormality is detected, the integrity monitoring system should provide a PL for bounding the absolute position error according to specified integrity risk. The integrity monitoring result is declared available only when the PL is less than the AL.

The Chi-squared residual-based RAIM is based on WLS positioning. In the GNSS WLS positioning, the linearized pseudorange equation with n measurements and m states can be expressed in the local ENU (East, North, Up) coordinate system as follows:

$$z = Hp + v + Ff_s + b_s \tag{1}$$

where z is the $n \times 1$ measurement vector, H is the $n \times m$ geometry matrix, p is the $m \times 1$ state vector, v is the $n \times 1$ Gaussian measurement noise vector with zero mean and diagonal covariance matrix R, f_s is the $n_f \times 1$ fault vector with n_f indicating the number of occurred measurement faults, F is a $n \times n_f$ matrix projecting the measurement faults

onto the measurement vector, each column and each row of F have at most one nonzero element with a value of 1, b_s is a $n \times 1$ vector indicating nominal biases and the nominal bias for satellite i is bounded by $b_{\text{norm},i}$.

As the f_s is a random vector, we rewrite (1) as follows:

$$z = Hp + v + Ff + Bb \tag{2}$$

where $f = f_s + F^T b_s$, b is a $\left(n - n_f\right) \times 1$ vector constructed by the nominal biases excluding the elements of $F^T b_s$, and B is a $n \times \left(n - n_f\right)$ matrix projecting b onto the measurement vector.

The WLS estimate of p is given as

$$\hat{p} = \left(H^T W H\right)^{-1} H^T W z \tag{3}$$

where $W = R^{-1}$ is the weighting matrix. Denoting $S = \left(H^T W H\right)^{-1} H^T W$, the WLS positioning error is equal to

$$\Delta p = \hat{p} - p = S(v + Ff + Bb) \tag{4}$$

and the covariance $\aleph$ of Δp is obtained by $\aleph = \left(H^T W H\right)^{-1}$. The residual vector of WLS is given by the following

$$r = z - H\hat{p} = (I - HS)(v + Ff + Bb) \tag{5}$$

Both Δp and r have normal distributions, respectively, expressed as

$$\Delta p \sim N\left(\Delta\overline{p} = S(Ff + Bb), \aleph\right) \tag{6}$$

$$r \sim N\left(\overline{r} = (I - HS)(Ff + Bb), (I - HS)R\right) \tag{7}$$

The weighted sum of squares of r is defined by

$$\chi^2 = r^T W r = z^T W (I - HS) z \tag{8}$$

If $\overline{r} = 0$, χ^2 follows a Chi-square distribution with $d = n - m$ degrees of freedom (Joerger and Pervan 2016); otherwise, χ^2 will follow a noncentral Chi-square distribution with d degrees of freedom and the noncentrality parameter is equal to

$$\lambda = (Ff + Bb)^T W (I - HS)(Ff + Bb) \tag{9}$$

In the Chi-squared residual-based RAIM, the test statistic for fault detection can be defined as $\alpha = \chi^2$. The threshold T_{th} of the test statistic then is computed by solving the following equation:

$$1 - P_{\text{FA}} = g_{\text{c}}\left(T_{\text{th}}\right) \tag{10}$$

where P_{FA} is the given probability of false alarm indicating the continuity requirement of the application and $g_{\text{c}}(*)$ is the cumulative distribution function of Chi-square distribution.

The PL calculation is related to specific fault detection method and the integrity risk requirement, which is determined by the following (Joerger and Pervan 2016)

$$\sum_{j=0}^{n_h} \left(P\left\{ \|\text{PE}\| > \text{PL}, \alpha < T_{\text{th}} | \hbar_j \right\} P_{\hbar_j} \right) \le P_{\text{HMI}} - P_{\text{NM}} \tag{11}$$

where PE can be either HPE or vertical position error (VPE), and corresponding PL is HPL or VPL, $\hbar_j$ with $0 \le j \le n_h$ represents an event hypothesis, $\hbar_0$ is the fault-free hypothesis, n_h is the number of events that should be monitored, $P_{\hbar_j}$ is the a priori probability of $\hbar_j$ occurrence, P_{HMI} is the probability of hazardously misleading information (HMI) indicating the integrity risk requirement and P_{NM} is the threshold for the integrity risk coming from very rarely occurring faults that need not be monitored. Since the Δp and α are statistically independent in GNSS WLS positioning (Sturza 1988; Joerger and Pervan 2013; Pervan 1996), equation (11) can be rewritten into

$$\sum_{j=0}^{n_h} \left(P\left\{ \|\text{PE}\| > \text{PL} | \hbar_j \right\} P\left\{ \alpha < T_{th} | \hbar_j \right\} P_{\hbar_j} \right) \le P_{HMI} - P_{NM} \tag{12}$$

The faults contained in fault event hypothesis $\hbar_j$ are indicated by matrix F as

$$\left\| F_{i,:} \right\| = \begin{cases} 1, & \text{fault in satellite } i \\ 0, & \text{no fault in satellite } i \end{cases} ; 1 \le i \le n \tag{13}$$

where $F_{i,:}$ is the i th row of F and $\|*\|$ means the matrix norm. Labeling the a priori probability of fault occurrence in GNSS satellite i as $P_{\text{sat},i}$ and considering that the GNSS faults (not include constellation faults) are independent of each other, the a priori probability of event hypothesis $\hbar_j$ (not include constellation faults) is equal to

$$P_{\hbar_j} = \begin{cases} \prod_{i=1}^{n} \left(1 - P_{\text{sat},i}\right) & ; j = 0 \\ \prod_{i=1}^{n} \left(\left(1 - P_{\text{sat},i}\right)^{1 - \left\| F_{i,:} \right\|} \left(P_{\text{sat},i}\right)^{\left\| F_{i,:} \right\|} \right) & ; j \ge 1 \end{cases} \tag{14}$$

The a priori probability of a GNSS constellation fault is specified in the integrity monitoring rather than calculated by (14) (Blanch et al. 2015).

Proposed HPL calculation for Chi-squared residual-based ARAIM

On the left side of (12), the probability $P\left\{\alpha < T_{th} | \hbar_j\right\}$ in each fault event hypothesis is affected by the noncentrality parameter, and the term $P\left\{\|\text{PE}\| > \text{PL} | \hbar_j\right\}$ is influenced by the PE distribution center. Both the PE distribution center and the noncentrality parameter are related to the fault vector as shown in (6) and (9). Since the fault vector is unknown in practice, the integrity monitoring algorithm should provide

a PL that can bound the PE occurred in the worst situation, which means the sum of the probability $P\{\|\mathrm{PE}\| > \mathrm{PL}|\hbar_j\}P\{\alpha < T_{th}|\hbar_j\}P_{\hbar_j}$ maximized by the worst PE distribution center and the worst noncentrality parameter in each event hypothesis should be less the integrity budget. In order to achieve a tight and reliable PL, it is required to determine the worst PE distribution center and the worst noncentrality parameter for each fault hypothesis. In the following part of this paper, we take the calculation of HPL as an example.

Bounding the HPE distribution center

Denoting the linearized pseudorange equation (2) in the fault event hypothesis $\hbar_j$ with $1 \le j \le n_h$ as $z = Hp + v + F_j f_j + B_j b_j$, then the PE distribution center and the noncentrality parameter can be expressed as follows:

$$\Delta\overline{p} = S\left(F_j f_j + B_j b_j\right) \tag{15}$$

$$\lambda_j = \left(F_j f_j + B_j b_j\right)^T W(I - HS)\left(F_j f_j + B_j b_j\right) \tag{16}$$

We define two variables as

$$\lambda_{f,j} = \left(F_j f_j\right)^T W(I - HS)\left(F_j f_j\right) \tag{17}$$

$$\lambda_{b,j} = \left(B_j b_j\right)^T W(I - HS) B_j b_j \tag{18}$$

The $\lambda_{f,j}$ represents the noncentrality parameter caused by the GNSS faults and nominal biases in faulty measurements, while the $\lambda_{b,j}$ stands for the noncentrality parameter only resulted by the nominal biases in fault-free measurements.

Defining Δp_{EN} as the horizontal GNSS WLS positioning error with subscripts E and N, respectively, indicating the east and north directions, we have

$$\Delta p_{\mathrm{EN}} = \left[x, y\right]^{\mathrm{T}} = C\Delta p \tag{19}$$

where x and y represent the coordinates along east and north directions in the horizontal plane, respectively, and C is the matrix to extract the horizontal elements from Δp. Then, the mean and covariance of Δp_{EN} can be, respectively, formulated as

$$\Delta\overline{p}_{\mathrm{EN}} = CS\left(F_j f_j + B_j b_j\right) \tag{20}$$

$$\aleph_{\mathrm{EN}} = C\aleph C^{\mathrm{T}} = UDU^{\mathrm{T}} \tag{21}$$

The UDU^{T} given in (21) is a singular value decomposition, and U is an orthogonal matrix and $D = \mathrm{diag}\left(\sigma_e, \sigma_n\right)$ composed of singular values is a diagonal matrix with $\sigma_e \ge \sigma_n$.

Every HPL derived from (12) protects the HPE under event hypothesis $\hbar_j$ within a circular region at the probability of $P\left\{\|\mathrm{HPE}\| \le \mathrm{HPL}|\hbar_j\right\}$, and the contour of the circular double integral region of $P\left\{\|\mathrm{HPE}\| \le \mathrm{HPL}|\hbar_j\right\}$ can be expressed in the horizontal plane as

$$\Delta p_{\mathrm{EN}}^{\mathrm{T}} \Delta p_{\mathrm{EN}} = \mathrm{HPL}^2 \tag{22}$$

The HPE along the east and north directions may be correlated with each other. In order to get an uncorrelated HPE, we take a coordinate transformation shown as follows:

$$\Delta p'_{\mathrm{EN}} = \left[x', y'\right]^{\mathrm{T}} = D^{-\frac{1}{2}} U^{\mathrm{T}} \Delta p_{\mathrm{EN}} \tag{23}$$

Then, the HPE in the new space is represented by $\Delta p'_{\mathrm{EN}}$ which has a unit covariance. The contour of the double integral region of $P\left\{\|\mathrm{HPE}\| \le \mathrm{HPL}|\hbar_j\right\}$ turns into an ellipse in the new space as follows:

$$\left(UD^{\frac{1}{2}} \Delta p'_{\mathrm{EN}}\right)^{\mathrm{T}} UD^{\frac{1}{2}} \Delta p'_{\mathrm{EN}} = \Delta p'^{\mathrm{T}}_{\mathrm{EN}} D \Delta p'_{\mathrm{EN}} = \mathrm{HPL}^2 \tag{24}$$

The HPE distribution center changes to

$$\Delta\overline{p'}_{\mathrm{EN}} = D^{-\frac{1}{2}} U^T CS\left(F_j f_j + B_j b_j\right) = \Delta\overline{p'}_{\mathrm{EN},f} + \Delta\overline{p'}_{\mathrm{EN},b} \tag{25}$$

where $\Delta\overline{p'}_{\mathrm{EN},f} = D^{-\frac{1}{2}} U^{\mathrm{T}} CSF_j f_j$ and $\Delta\overline{p'}_{\mathrm{EN},b} = D^{-\frac{1}{2}} U^T CSB_j b_j$, respectively, represent the HPE caused by f_j and b_j.

Bound for the HPE caused by faults

We assume that

$$F_j^T W(I - HS)F_j = U_1 D_1 U_1^T \tag{26}$$

where $U_1 D_1 U_1^T$ is a singular value decomposition, and U_1 is an orthogonal matrix and $D_1 = \mathrm{diag}\left(\varepsilon_1, \varepsilon_2, \ldots, \varepsilon_{n_D}, 0_{1\times(n_f - n_D)}\right)$ composed of singular values is a diagonal matrix with n_D=rank$\left(D_1\right)$ and $\varepsilon_1 \ge \varepsilon_2 \ge \cdots \ge \varepsilon_{n_D}$. Then, we perform a coordinate transformation as

$$f'_j = D_f U_1^T f_j \tag{27}$$

where $D_f = \mathrm{diag}\left(\sqrt{\varepsilon_1}, \sqrt{\varepsilon_2}, \ldots, \sqrt{\varepsilon_{n_D}}, 1_{1\times(n_f - n_D)}\right)$. As a result, $\lambda_{f,j} = \left(F_j f_j\right)^{\mathrm{T}} W(I - HS)\left(F_j f_j\right)$ and $\Delta\overline{p'}_{\mathrm{EN},f} = D^{-\frac{1}{2}} U^T CSF_j f_j$ become $\lambda_{f,j} = \left(f'_j\right)^{\mathrm{T}} \mathrm{diag}\left(1_{1\times n_D}, 0_{1\times(n_f - n_D)}\right) f'_j$ and $\Delta\overline{p'}_{\mathrm{EN},f} = D^{-\frac{1}{2}} U^T CSF_j U_1 D_f^{-1} f'_j$, respectively.

Assume that we have the following singular value decomposition

$$\begin{aligned}&\left(D^{-\frac{1}{2}} U^T CSF_j U_1 D_f^{-1}\right)^T D^{-\frac{1}{2}} U^T CSF_j U_1 D_f^{-1} \\ &= U_2 \mathrm{diag}\left(\varsigma_1, \varsigma_2, 0_{1\times(n_f - 2)}\right) U_2^T\end{aligned} \tag{28}$$

where U_2 is an orthogonal matrix and $\varsigma_1 \geq \varsigma_2$. Based on the covariance ellipsoid concept and the consistency relationship between two covariance ellipsoids (Benaskeur 2002; Liu et al. 2017), the HPE induced by GNSS faults under a given $\lambda_{f,j}$ in the new space is bounded by

$$\left\|\Delta\overline{p'}_{\mathrm{EN},f}\right\| \leq \sqrt{\lambda_{f,j}\varsigma_1} \tag{29}$$

Similarly, we denote $D_r = [1, 0]$ and assume the following singular value decomposition

$$\begin{aligned}&\left(D_r D^{-\frac{1}{2}} U^T \mathrm{CSF}_j U_1 D_f^{-1}\right)^T D_r D^{-\frac{1}{2}} U^T \mathrm{CSF}_j U_1 D_f^{-1} \\ &= U_3 \mathrm{diag}\left(\xi_1, 0_{1\times(n_f-1)}\right) U_3^T\end{aligned} \tag{30}$$

where U_3 is an orthogonal matrix. The magnitude of the HPE induced by GNSS faults along x_{f}-axis under a given $\lambda_{f,j}$ in the new space is bounded by

$$\left|x_f\right| \leq \sqrt{\lambda_{f,j}\xi_1} \tag{31}$$

Getting the bounds of $\left\|\Delta\overline{p'}_{\mathrm{EN},f}\right\|$ and $\left|x'_f\right|$ can be considered to solve optimization problems that have linear or quadratic objectives and quadratic equality constraints, which can also be settled by optimization methods. The upper bound of the HPE caused by a constellation fault can be similarly calculated.

Bound for the HPE caused by nominal biases

Again, we assume the following singular value decomposition

$$\begin{aligned}&\left(D^{-\frac{1}{2}} U^T CSB_j\right)^T D^{-\frac{1}{2}} U^T CSB_j \\ &= U_4 \mathrm{diag}\left(\zeta_1, \zeta_2, \ldots, \zeta_{n-n_f}\right) U_4^T\end{aligned} \tag{32}$$

where U_4 is an orthogonal matrix and $\zeta_1 \geq \zeta_2 \geq \cdots \geq \zeta_{n-n_f}$. Then, the HPE induced by b_j in the new space is bounded by

$$\left\|\Delta\overline{p'}_{\mathrm{EN},b}\right\| \leq \sqrt{\zeta_1 \sum_{i=1}^{n}\left(\left\|B_{j,i,:}\right\| b^2_{\mathrm{norm},i}\right)} \tag{33}$$

The magnitude of the HPE induced by b_j along $\mathrm{x_f}$-axis in the new space is bounded by

$$\left|x'_b\right| \leq \sum_{i=1}^{n}\left(\left|e_i\right|\left\|B_{j,i,:}\right\| b_{\mathrm{norm},i}\right) \tag{34}$$

where e_i is the i th element of $D_r D^{-\frac{1}{2}} U^T CS$.

The double integral of $P\left\{\|\mathrm{HPE}\| \leq \mathrm{HPL}|\hbar_j\right\}$ in the new space is graphically shown in Fig. 1, and we have two lemmas as follows:

Lemma 1 *For any two points P_A, P_B in a horizontal line (or two points P_A, P_C in a vertical line), the double integral of $P\left\{\|\mathrm{HPE}\| \leq \mathrm{HPL}|\hbar_j\right\}$ with the HPE distribution center at the point P_B which is closer to the y'-axis (or at the point P_C which is closer to the x'-axis) has a greater value (proof is given in Appendix A): $P\left\{\|\mathrm{HPE}\| \leq \mathrm{HPL}|\hbar_j, P_B\right\} > P\left\{\|\mathrm{HPE}\| \leq \mathrm{HPL}|\hbar_j, P_A\right\}$ (or $P\left\{\|\mathrm{HPE}\| \leq \mathrm{HPL}|\hbar_j, P_C\right\} > P\left\{\|\mathrm{HPE}\| \leq \mathrm{HPL}|\hbar_j, P_A\right\}$).*

Lemma 2 *For any two points P_D, P_E in a circular arc whose center is at the origin, the double integral of $P\left\{\|\mathrm{HPE}\| \leq \mathrm{HPL}|\hbar_j\right\}$ with the HPE distribution center at the point P_E which is closer to the y'-axis has a greater value (proof is given in Appendix B): $P\left\{\|\mathrm{HPE}\| \leq \mathrm{HPL}|\hbar_j, P_E\right\} > P\left\{\|\mathrm{HPE}\| \leq \mathrm{HPL}|\hbar_j, P_D\right\}$.*

Since the double integral of $P\left\{\|\mathrm{HPE}\| \leq \mathrm{HPL}|\hbar_j\right\}$ in the new space is symmetric about the x'-axis and the y'-axis, without loss of generality we assume the worst HPE distribution center in the new space is in the first quadrant. Define the following line and circle in the new space

$$x' = \max\left(x'_f\right) + \max\left(x'_b\right) \tag{35}$$

$$x'^2 + y'^2 = \left(\max\left(\left\|\Delta\overline{p'}_{\mathrm{EN},f}\right\|\right) + \max\left(\left\|\Delta\overline{p'}_{\mathrm{EN},b}\right\|\right)\right)^2 \tag{36}$$

The HPE distribution center in the first quadrant can be at any point in the grid area in Fig. 1. According to the two lemmas, the upper bound of the worst HPE distribution center caused by both faults and nominal biases in the new space

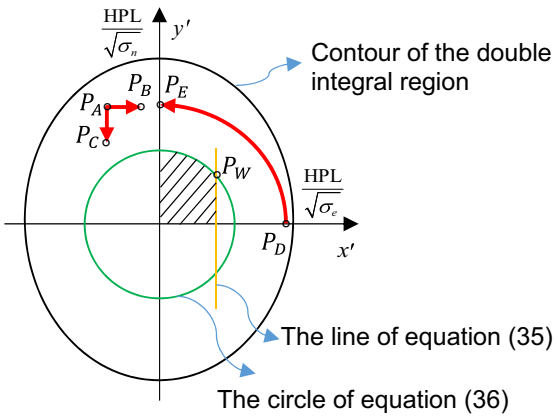

Fig. 1 Double integral of $P\left\{\|\mathrm{HPE}\| \leq \mathrm{HPL}|\hbar_j\right\}$ in the new space

can be represented by the intersection $P_{\mathrm{W}} = \left[\mu_{x',w}, \mu_{y',w}\right]^{\mathrm{T}}$ of the orange line and the green circle in Fig. 1.

Based on the obtained upper bound of the worst HPE distribution center in the new space, we have

$$\begin{aligned} &P\left\{\|\mathrm{HPE}\| > \mathrm{HPL}|\hbar_j, \lambda_{f,j}\right\} \\ &\le \left(1 - P\left\{\|\mathrm{HPE}\| \le \mathrm{HPL}|\hbar_j, \lambda_{f,j}, \mu_{x',w}, \mu_{y',w}\right\}\right) \end{aligned} \tag{37}$$

where $P\left\{\|\mathrm{HPE}\| \le \mathrm{HPL}|\hbar_j, \lambda_{f,j}, \mu_{x',w}, \mu_{y',w}\right\}$ means the probability $P\left\{\|\mathrm{HPE}\| \le \mathrm{HPL}|\hbar_j\right\}$ under the given $\lambda_{f,j}$ with the upper bound of the worst HPE distribution center at $\left[\mu_{x',w}, \mu_{y',w}\right]^{\mathrm{T}}$, and

$$\begin{aligned} &P\left\{\|\mathrm{HPE}\| \le \mathrm{HPL}|\hbar_j, \lambda_{f,j}, \mu_{x',w}, \mu_{y',w}\right\} \\ &= \int_{-\frac{\mathrm{HPL}}{\sqrt{\sigma_e}}}^{\frac{\mathrm{HPL}}{\sqrt{\sigma_e}}} \mathrm{d}x' \int_{-\sqrt{\frac{\mathrm{HPL}^2}{\sigma_n} - \frac{\sigma_e}{\sigma_n}x'^2}}^{\sqrt{\frac{\mathrm{HPL}^2}{\sigma_n} - \frac{\sigma_e}{\sigma_n}x'^2}} \frac{1}{2\pi} e^{-\frac{1}{2}\left((x'-\mu_{x',w})^2 + (y'-\mu_{y',w})^2\right)} \mathrm{d}y' \end{aligned} \tag{38}$$

As for VPL calculation, the upper bound of the worst VPE distribution center caused by both GNSS faults and nominal biases is represented by the max(y) in the original space, which can be obtained by a way similar to (29) (31), (33), (34) and (35) used to achieve the $\max\left(x'\right)$.

Bounding the noncentrality parameter

Here, the worst HPE distribution center in the new space is still assumed in the first quadrant. For the fault event hypothesis $\hbar_j$ with $1 \le j \le n_h$, we assume the following singular value decomposition:

$$B_j^T W(I - HS)B_j = U_5 \mathrm{diag}\left(\gamma_1, \gamma_2, \ldots, \gamma_{n-n_f}\right) U_5^T \tag{39}$$

where U_5 is an orthogonal matrix and $\gamma_1 \ge \gamma_2 \ge \cdots \ge \gamma_{n-n_f}$. Then, we have

$$\begin{aligned} &\lambda_{b,j} = \left(B_j b_j\right)^T W(I - HS)B_j b_j \\ &\le \lambda_{b,j}^{\max} = \gamma_1 \sum_{i=1}^{n} \left(\left\|B_{j,i,:}\right\| b_{\mathrm{norm},i}^2\right) \end{aligned} \tag{40}$$

According to the definitions of λ_j, $\lambda_{f,j}$ and $\lambda_{b,j}$, we have the following

$$\lambda_j \ge \left(\sqrt{\lambda_{f,j}} - \sqrt{\lambda_{b,j}}\right)^2 \tag{41}$$

We define the following function:

$$q\left(\hbar_j, \lambda_{f,j}\right) = \begin{cases} P\left\{\alpha < T_{\mathrm{th}}|\hbar_j, 0\right\} & ;\lambda_{f,j} < \lambda_{b,j}^{\max} \\ P\left\{\alpha < T_{\mathrm{th}}|\hbar_j, \left(\sqrt{\lambda_{f,j}} - \sqrt{\lambda_{b,j}^{\max}}\right)^2\right\} & ;\lambda_{f,j} \ge \lambda_{b,j}^{\max} \end{cases} \tag{42}$$

where $P\left\{\alpha < T_{\mathrm{th}}|\hbar_j, \lambda\right\}$ means the probability $P\left\{\alpha < T_{\mathrm{th}}|\hbar_j\right\}$ when the noncentrality parameter of the noncentral Chi-square distribution of test statistic is equal to λ. As shown in (41), $\lambda_j \ge \left(\sqrt{\lambda_{f,j}} - \sqrt{\lambda_{b,j}}\right)^2 \ge 0$. Hence, $P\left\{\alpha < T_{th}|\hbar_j, \lambda_j\right\} \le P\left\{\alpha < T_{th}|\hbar_j, \left(\sqrt{\lambda_{f,j}} - \sqrt{\lambda_{b,j}}\right)^2\right\} \le q\left(\hbar_j, \lambda_{f,j}\right)$. Then, according to (37), for any $\lambda_{f,j}$ with corresponding obtained upper bound of the worst HPE distribution center at $\left[\mu_{x',w}, \mu_{y',w}\right]^T$, each term on the left side of (12) for the fault event hypothesis $\hbar_j$ with $1 \le j \le n_h$ can expressed as

$$\begin{aligned} P_{\mathrm{HMI},j} &= P\left\{\|\mathrm{HPE}\| > \mathrm{HPL}|\hbar_j\right\} P\left\{\alpha < T_{th}|\hbar_j, \lambda_j\right\} P_{\hbar_j} \\ &\le \left(1 - P\left\{\|\mathrm{HPE}\| \le \mathrm{HPL}|\hbar_j, \lambda_{f,j}, \mu_{x',w}, \mu_{y',w}\right\}\right) \\ &\quad \times P\left\{\alpha < T_{th}|\hbar_j, \lambda_j\right\} P_{\hbar_j} \\ &\le \hat{P}_{\mathrm{HMI},j} = \left(1 - P\left\{\|\mathrm{HPE}\| \le \mathrm{HPL}|\hbar_j, \lambda_{f,j}, \mu_{x',w}, \mu_{y',w}\right\}\right) \\ &\quad \times q\left(\hbar_j, \lambda_{f,j}\right) P_{\hbar_j} \end{aligned} \tag{43}$$

Inequality (43) indicates $P_{\mathrm{HMI},j}^{\max} = \max\left(P_{\mathrm{HMI},j}\right) \le \hat{P}_{\mathrm{HMI},j}^{\max} = \max\left(\hat{P}_{\mathrm{HMI},j}\right)$. Hence, $P_{\mathrm{HMI},j}$ is bounded by $\hat{P}_{\mathrm{HMI},j}^{\max}$ for the given $\lambda_{f,j}$.

Bounding the integrity risk

Given a HPL candidate, $\hat{P}_{HMI,j}$ is a function of $\lambda_{f,j}$. In order to achieve the $\hat{P}_{\mathrm{HMI},j}^{\max}$, we should find the worst $\lambda_{f,j}$. The $\lambda_{f,j}$ is related to the magnitudes of the faults contained in the fault event hypothesis $\hbar_j$, and each fault magnitude in the fault event can vary from 0 to a large unknown value. It can be very computationally costly to search the worst $\lambda_{f,j}$ in the range $\lambda_{f,j} \in (0, +)$ along with the double integral given in (38) in the ellipse region defined by (24) for each fault event hypothesis.

As shown in Fig. 2, we use ○ to denote the double integral region of $P\left\{\|\mathrm{HPE}\| \le \mathrm{HPL}|\hbar_j\right\}$, and employ $\square_{in}$ to indicate the inscribed rectangle (can be constructed by different ways) of ○.

Also, we define the following functions:

$$\begin{aligned} &p\left(\hbar_j, \diamond, \lambda_{f,j}\right) = P\left\{\mathrm{HPE} \in \diamond|\hbar_j, \lambda_{f,j}, \mu_{x',w}, \mu_{y',w}\right\} \\ &= \iint_{\diamond} \frac{1}{2\pi} e^{-\frac{1}{2}\left((x'-\mu_{x',w})^2 + (y'-\mu_{y',w})^2\right)} dx'dy' \end{aligned} \tag{44}$$

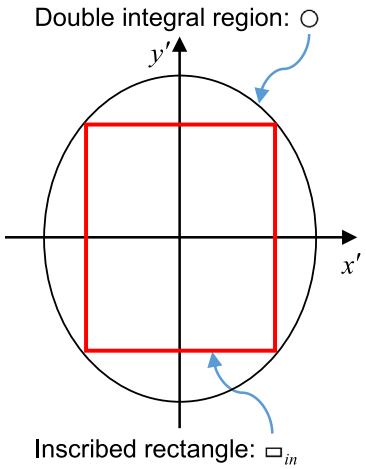

Fig. 2 Inscribed rectangle of the double integral region

$$g(\hbar_j, \diamondsuit, \lambda_{f,j}) = (1 - p(\hbar_j, \diamondsuit, \lambda_{f,j}))q(\hbar_j, \lambda_{f,j})P_{\hbar_j} \tag{45}$$

where $\diamondsuit \subset \{\bigcirc, \square_{in}\}$ (which means $\diamondsuit$ can be $\bigcirc$ or $\square_{in}$). Compared to $g(\hbar_j, \bigcirc, \lambda_{f,j})$ whose integral region is an ellipse, the $g\left(\hbar_j, \square_{in}, \lambda_{f,j}\right)$ has a rectangular integral region. The double integral with a rectangle region $x_L \le x \le x_U, y_L \le y \le y_U$ of the two-dimensional normal distribution $[x, y]^{\mathrm{T}} \sim N\left([\mu_x, \mu_y]^{\mathrm{T}}, \mathrm{diag}(\sigma_x, \sigma_y)\right)$ can be efficiently calculated using the error function as follows:

$$\begin{aligned}
&\int_{x_L}^{x_U} \mathrm{d}x \int_{y_L}^{y_U} \frac{1}{2\pi\sigma_x\sigma_y} e^{-\frac{1}{2}\left(\left(\frac{x-\mu_x}{\sigma_x}\right)^2 + \left(\frac{y-\mu_y}{\sigma_y}\right)^2\right)} \mathrm{d}y \\
&= \frac{1}{4}\left(\mathrm{erf}\left(\frac{\mu_x - x_L}{\sqrt{2}\sigma_x}\right) - \mathrm{erf}\left(\frac{\mu_x - x_U}{\sqrt{2}\sigma_x}\right)\right) \\
&\quad \times \left(\mathrm{erf}\left(\frac{\mu_y - y_L}{\sqrt{2}\sigma_y}\right) - \mathrm{erf}\left(\frac{\mu_y - y_U}{\sqrt{2}\sigma_y}\right)\right)
\end{aligned} \tag{46}$$

where $\mathrm{erf}(*)$ is the error function expressed as follows:

$$\mathrm{erf}(t) = \frac{2}{\sqrt{\pi}} \int_0^t e^{-s^2} \mathrm{d}s \tag{47}$$

We assume that $g\left(\hbar_j, \square_{in}, \lambda_{f,j}\right)$ and $g(\hbar_j, \bigcirc, \lambda_{f,j})$ are maximized at $\lambda_{f,j} = \lambda_{max,j}^{\square_{in}}$ and $\lambda_{f,j} = \lambda_{\max,j}^{\bigcirc}$, respectively. Based on the definition in (45), we have $\hat{P}_{\mathrm{HMI},j} = g(\hbar_j, \bigcirc, \lambda_{f,j})$ and $\hat{P}_{\mathrm{HMI},j}^{\max} = g\left(\hbar_j, \bigcirc, \lambda_{\max,j}^{\bigcirc}\right)$. Because $\square_{in}$ is contained within $\bigcirc$, we have $g\left(\hbar_j, \bigcirc, \lambda_{max,j}^{\bigcirc}\right) < g\left(\hbar_j, \square_{in}, \lambda_{max,j}^{\bigcirc}\right) < g\left(\hbar_j, \square_{in}, \lambda_{max,j}^{\square_{in}}\right)$. Hence, $P_{HMI,j}^{\max} \le \hat{P}_{HMI,j}^{\max} < g\left(\hbar_j, \square_{in}, \lambda_{max,j}^{\square_{in}}\right)$. The upper bound $P_{\mathrm{HMI},j}^{\mathrm{up}}$ for $P_{\mathrm{HMI},j}$ can be obtained as

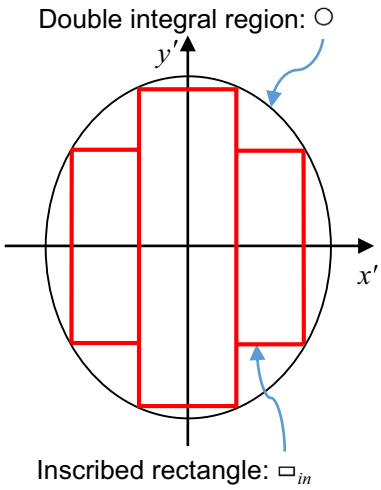

Fig. 3 Double integral with multiple rectangles

$$P_{HMI,j}^{up} = g\left(\hbar_j, \square_{in}, \lambda_{max,j}^{\square_{in}}\right) \tag{48}$$

To reduce the difference between $g\left(\hbar_j, \square_{in}, \lambda_{max,j}^{\square_{in}}\right)$ and $g\left(\hbar_j, \bigcirc, \lambda_{\max,j}^{\bigcirc}\right)$, the inscribed rectangle $\square_{in}$ can be further replaced by multiple smaller rectangles as shown in Fig. 3.

In order to get $g\left(\hbar_j, \square_{in}, \lambda_{max,j}^{\square_{in}}\right)$, the $\lambda_{max,j}^{\square_{in}}$ is required to be determined. The $\lambda_{max,j}^{\square_{in}}$ can be obtained by search method. In the searching of $\lambda_{max,j}^{\square_{in}}$, the lower bound $\lambda_{f,j}^{\mathrm{low}}$ and upper bound $\lambda_{f,j}^{\mathrm{up}}$ of $\lambda_{f,j}$ should be first determined and the searching can start at the upper bound $\lambda_{f,j}^{\mathrm{up}}$. The lower bound is set as $\lambda_{f,j}^{\mathrm{low}} = \lambda_{b,j}^{\max}$, and a conservative upper bound ($\lambda_{f,j}^{\mathrm{up}} \ge \lambda_{b,j}^{\max}$) can be obtained by solving the following:

$$q\left(\hbar_j, \lambda_{f,j}^{up}\right) = \frac{g\left(\hbar_j, \square_{in}, \lambda_{b,j}^{\max}\right)}{P_{\hbar_j}} \tag{49}$$

Then, we have

$$\begin{aligned}
&g\left(\hbar_j, \square_{in}, \lambda_{f,j}\right) \\
&= \left(1 - p\left(\hbar_j, \square_{in}, \lambda_{f,j}\right)\right) q\left(\hbar_j, \lambda_{f,j}\right) P_{\hbar_j} \\
&\le \left(1 - p\left(\hbar_j, \square_{in}, \lambda_{f,j}\right)\right) g\left(\hbar_j, \square_{in}, \lambda_{b,j}^{\max}\right) \\
&< g\left(\hbar_j, \square_{in}, \lambda_{b,j}^{\max}\right)
\end{aligned} \quad ; \text{when } \lambda_{f,j} \ge \lambda_{f,j}^{up} \tag{50}$$

The above inequality implies that we do not need to search the range $\lambda_{f,j} > \lambda_{f,j}^{\mathrm{up}}$. In practice, $\lambda_{max,j}^{\square_{in}}$ is usually much smaller than the $\lambda_{f,j}^{\mathrm{up}}$.

Since the error function can be pre-implemented, the $p\left(\hbar_j, \square_{in}, \lambda_{f,j}\right)$ can be more efficiently computed than $p(\hbar_j, \bigcirc, \lambda_{f,j})$. Compared to searching $\lambda_{\max,j}^{\bigcirc}$ in the range

$\lambda_{f,j} \in (0,+)$ along with double integral, the proposed method using (48) to compute integrity risk not only has a narrow search range $\left[\lambda_{b,j}^{\max}, \lambda_{f,j}^{\mathrm{up}}\right]$ for $\lambda_{max,j}^{\square_{in}}$ but also can eliminate the double integral.

HPL calculation process

The proposed algorithm calculates the HPL following the main steps below, and the calculation flowchart is shown in Fig. 4:

1. Given a HPL, construct the inscribed rectangle(s) $\square_{in}$ in the new space.
2. Based on (45), compute the probability $P_{\mathrm{HMI},0}$ either using $g(\hbar_0, \bigcirc, 0)$ or $g(\hbar_0, \square_{in}, 0)$.
3. For each event hypothesis $\hbar_j$ with $1 \le j \le n_h$, search $\lambda_{max,j}^{\square_{in}}$ and then use (48) to obtain $P_{\mathrm{HMI},j}^{\mathrm{up}}$.
4. Check whether $\left(P_{\mathrm{HMI},0} + \sum_{j=1}^{n_h} P_{\mathrm{HMI},j}^{\mathrm{up}}\right) \le \left(P_{\mathrm{HMI}} - P_{\mathrm{NM}}\right)$ is satisfied and their difference is smaller than stop criterion. If the check does not pass, return to step 1 and continue the calculation with a new HPL candidate.

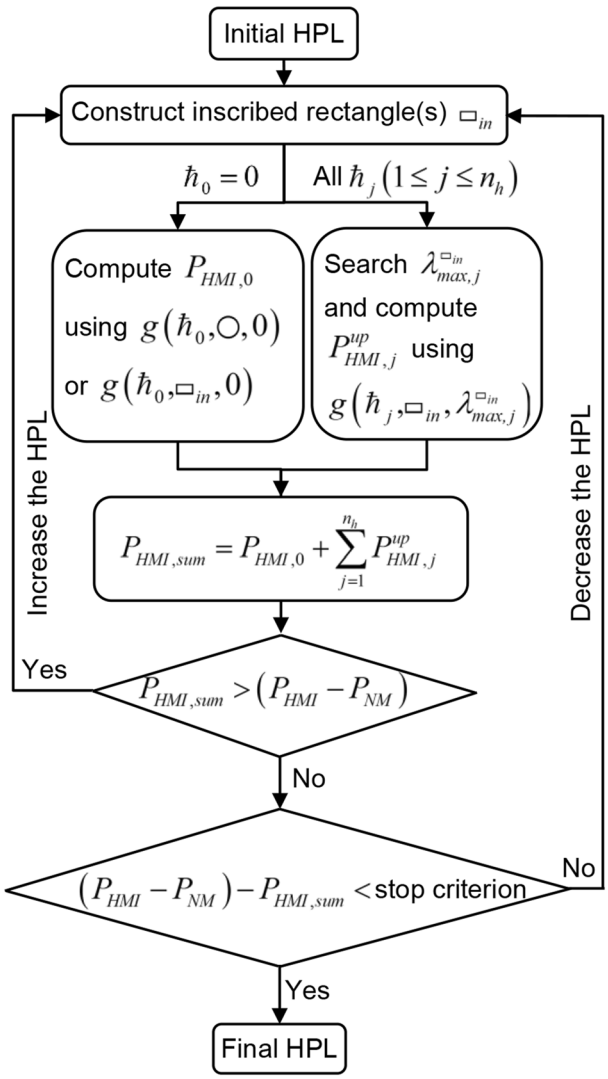

Fig. 4 HPL calculation flowchart

Note that in the continuous integrity monitoring, the search of $\lambda_{max,j}^{\square_{in}}$ at the current epoch can be conducted with the worst parameter obtained at the previous epoch as the initial value, such that the cost time of the HPL calculation will be further suppressed. When setting the initial HPL for the first iteration, we should be aware that the HPL has a lower bound. Rewrite the left side of (12) for HPL into

$$\begin{aligned}
&\sum_{j=0}^{n_h} \left(P\{\|\mathrm{HPE}\| > \mathrm{HPL}|\hbar_j\} P\{\alpha < T_{th}|\hbar_j\} P_{\hbar_j}\right) \\
&= P\{\|\mathrm{HPE}\| > \mathrm{HPL}|\hbar_0\} P\{\alpha < T_{th}|\hbar_0\} P_{\hbar_0} \\
&\quad + \sum_{j=1}^{n_h} \left(P\{\|\mathrm{HPE}\| > \mathrm{HPL}|\hbar_j\} P\{\alpha < T_{th}|\hbar_j\} P_{\hbar_j}\right) \\
&\le P_{\mathrm{HMI}} - P_{\mathrm{NM}}
\end{aligned} \tag{51}$$

When $\lambda_{\max,j}^{\bigcirc} \to \infty, 1 \le j \le h$, for any feasible HPL we have

$$P\{\|\mathrm{HPE}\| > \mathrm{HPL}|\hbar_0\} P\{\alpha < T_{\mathrm{th}}|\hbar_0\} P_{\hbar_0} \le P_{\mathrm{HMI}} - P_{\mathrm{NM}}. \tag{52}$$

Hence, equation (12) has a lower HPL bound as $\mathrm{HPL}_{\min}$ which satisfies

$$\begin{aligned}
&P\{\|\mathrm{HPE}\| > \mathrm{HPL}_{\min}|\hbar_0\} P\{\alpha < T_{\mathrm{th}}|\hbar_0\} P_{\hbar_0} \\
&= P_{\mathrm{HMI}} - P_{\mathrm{NM}}
\end{aligned} \tag{53}$$

In the VPL calculation, a similar lower bound for VPL also exists.

Experiment

In this section, an experiment based on GPS, Galileo and BDS ephemeris data is conducted to demonstrate the proposed algorithm. The broadcast GPS, Galileo and BDS ephemeris data on 2020–01-01 are downloaded from ftp://cddis.nasa.gov/gnss/data/campaign/mgex/daily/rinex3/2020/001/20p/ and used to construct the geometry matrix of GNSS WLS positioning at 2020-01-01, 22: 00 in ENU coordinate system. HPL calculation is performed with a fixed height of 1000 m and a horizontal interval of 10° in both latitude (−80° to 80°) and longitude (−170° to 180°). All-in-view satellites of those

three GNSS constellations with an elevation (degree) $\phi \geq 10°$ are applied.

We assume that the pseudorange of each satellite is measured by a dual-frequency receiver and its error variance represented by $R(i,i)$ is computed as follows:

$$R(i,i) = \sigma^2_{\mathrm{URA},i} + \sigma^2_{\mathrm{tropo},i} + \sigma^2_{\mathrm{user},i} \tag{54}$$

where $\sigma_{\mathrm{URA},i}$ is the standard deviation caused by satellite clock and ephemeris error and $\sigma_{\mathrm{tropo},i}$ and $\sigma_{\mathrm{user},i}$ are the standard deviations introduced by tropospheric delay and receiver, respectively. Both $\sigma_{\mathrm{tropo},i}$ and $\sigma_{\mathrm{user},i}$ are considered to be related to the satellite elevation and the models presented in (Blanch et al. 2015) are applied here.

$$\sigma_{\mathrm{user},i} = \sqrt{\frac{f_a^4 + f_b^4}{\left(f_a^2 + f_b^2\right)^2}} \times \sqrt{\left(0.13 + 0.53e^{-\frac{\phi}{10}}\right)^2 + \left(0.15 + 0.43e^{-\frac{\phi}{6.9}}\right)^2} \tag{55}$$

$$\sigma_{\mathrm{tropo},i} = \frac{0.12012}{\sqrt{0.002001 + \sin^2\left(\pi\phi/180\right)}} \tag{56}$$

where f_a and f_d are two frequencies used to measure pseudorange.

The main integrity monitoring parameters for horizontal mode are allocated as

$$P_{\mathrm{HMI}} - P_{\mathrm{NM}} = 1 \times 10^{-8}, P_{\mathrm{FA}} = 9 \times 10^{-8} \tag{57}$$

and for each constellation or satellite,

$$P_{\mathrm{const}} = 1 \times 10^{-5}, P_{\mathrm{sat},i} = 1 \times 10^{-4}$$
$$\sigma_{\mathrm{URA},i} = 1.0\,\mathrm{m}, b_{\mathrm{norm},i} = 0.5\,\mathrm{m} \tag{58}$$

P_{const} is the a prior probability of constellation fault. In the experiment, the $\square_{in}$ is constructed by 2000 small rectangles within semi-x-axis. Constellation fault, nominal biases and the fault event hypotheses with at most two simultaneous satellite faults are considered. The HPL achieved by the proposed algorithm is compared with that of SS-ARAIM whose HPL is computed by $\mathrm{HPL} = \sqrt{\mathrm{HPL}_e^2 + \mathrm{HPL}_n^2}$ with the subscripts e, n indicating the east, north PL components, respectively.

The number of used GPS, Galileo and BDS satellites is shown in Fig. 5, and the HPL obtained by the proposed algorithm is shown in Fig. 6. Compared to other faults, the constellation faults have a greater impact on the integrity and basically determine the retrievable level of HPL. Figure 7 shows the percentage of HPL improvement compared to SS-ARAIM. Although the HPL calculation of the proposed

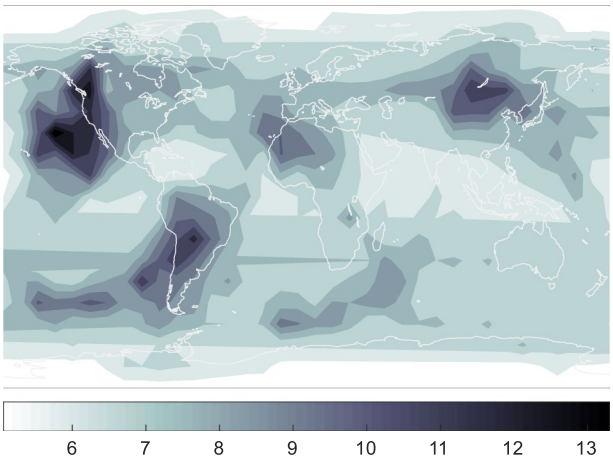

Fig. 6 HPL (meter) obtained by the proposed algorithm

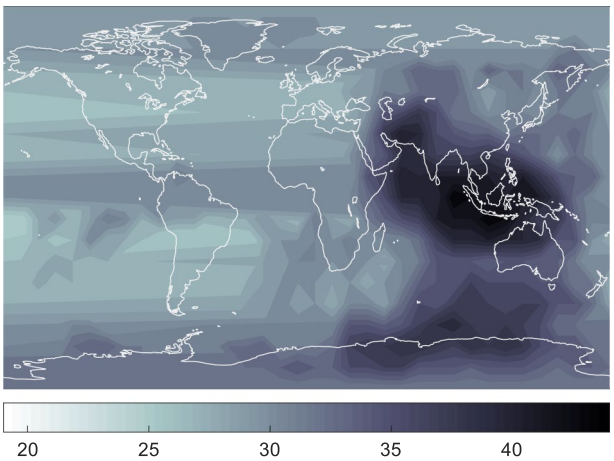

Fig. 5 Number of used satellites

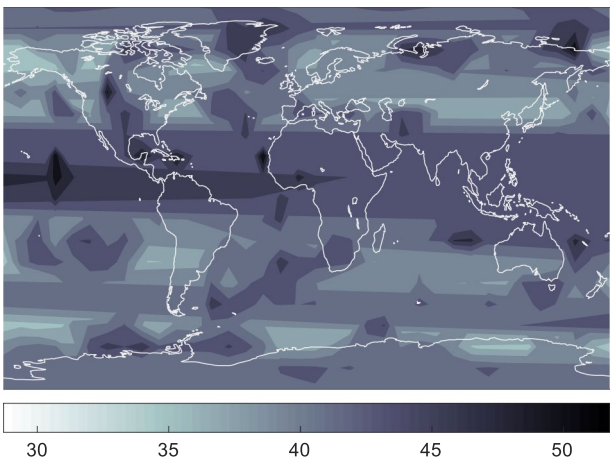

Fig. 7 Percentage (%) of HPL improvement compared to SS-ARAIM

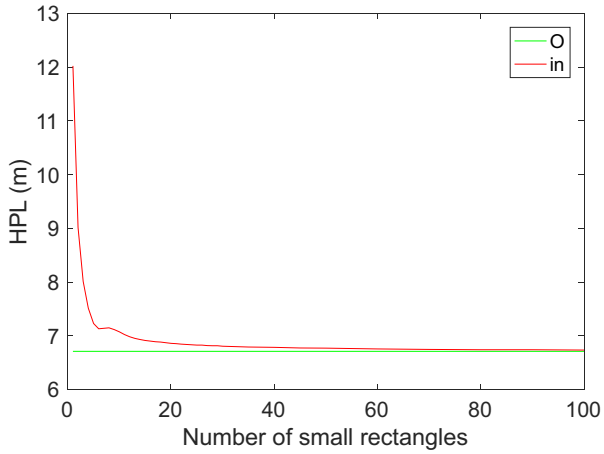

Fig. 8 HPL with respect to the number of the small rectangles used to construct $\square_{in}$ at the location with latitude = 0° and longitude = 0°

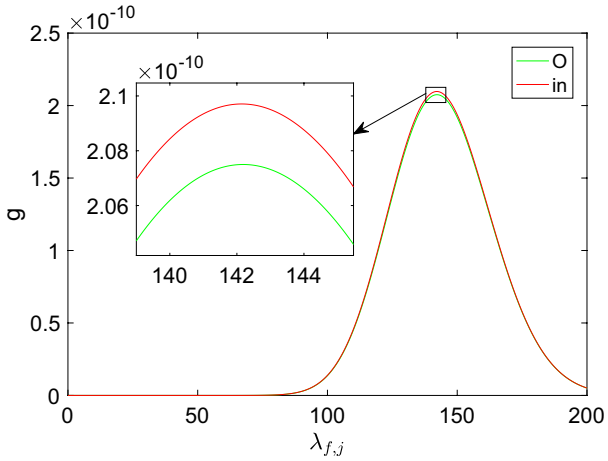

Fig. 9 Changes of $g\left(\hbar_j, \square_{in}, \lambda_{f,j}\right)$ and $g(\hbar_j, \bigcirc, \lambda_{f,j})$ with respect to $\lambda_{f,j}$ in GPS constellation fault event hypothesis at the location with latitude = 0° and longitude = 0°

algorithm is more complicated than that of SS-ARAIM, it can significantly improve the HPL tightness.

The construction of $\square_{in}$ affects the difference between $g\left(\hbar_j, \square_{in}, \lambda^{\square_{in}}_{max,j}\right)$ and $g\left(\hbar_j, \bigcirc, \lambda^{\bigcirc}_{\max,j}\right)$ and hence has an influence on the level of the conservativeness of the HPL computed using (48). For the location with latitude = 0° and longitude = 0°, the computed HPL with respect to the number of the small rectangles (within semi-x-axis) used to construct $\square_{in}$ is shown in Fig. 8. It can be seen from Fig. 8 that the HPL computed using (48) (the red curve) is more conservative than that the one achieved through searching $\lambda^{\bigcirc}_{\max,j}$ (the green curve). However, the computed HPL becomes tight quickly as the number of the small rectangles increases. The difference between the HPL obtained by (48) and searching $\lambda^{\bigcirc}_{\max,j}$ is less than 0.15 m when the $\square_{in}$ is constructed by 20 or more rectangles within semi-x-axis.

With the final obtained HPL, the changes of $g\left(\hbar_j, \square_{in}, \lambda_{f,j}\right)$ and $g(\hbar_j, \bigcirc, \lambda_{f,j})$ with respect to $\lambda_{f,j}$ in GPS constellation fault event hypothesis at the location with latitude=0° and longitude=0° are shown in Fig. 9. By constructing $\square_{in}$ with multiple small rectangles, the $\lambda^{\square_{in}}_{max,j}$ and $\lambda^{\bigcirc}_{\max,j}$ as well as the curves of $g\left(\hbar_j, \square_{in}, \lambda_{f,j}\right)$ and $g\left(\hbar_j, \bigcirc, \lambda_{f,j}\right)$ are both very close to each other. In Fig. 9, $\lambda^{\square_{in}}_{max,j}$, $\lambda^{\bigcirc}_{\max,j} = 142.19$ and $g\left(\hbar_j, \square_{in}, \lambda^{\square_{in}}_{max,j}\right) = 2.09707 \times 10^{-10}$, $g\left(\hbar_j, \bigcirc, \lambda^{\bigcirc}_{\max,j}\right) = 2.07499 \times 10^{-10}$. The difference between $g\left(\hbar_j, \square_{in}, \lambda^{\square_{in}}_{max,j}\right)$ and $g\left(\hbar_j, \bigcirc, \lambda^{\bigcirc}_{\max,j}\right)$ is far smaller than the integrity risk requirement. Figures 8 and 9 demonstrate that $g\left(\hbar_j, \square_{in}, \lambda^{\square_{in}}_{max,j}\right)$ instead of $g\left(\hbar_j, \bigcirc, \lambda^{\bigcirc}_{\max,j}\right)$ can be used to conservatively compute integrity risk in the HPL calculation as it will not cause an over conservativeness when the $\square_{in}$ is constructed by multiple rectangles.

Conclusions

This work proposes an algorithm to calculate the HPL of Chi-squared residual-based ARAIM. Since the HPE has a two-dimensional normal distribution, the HPL tightness can be improved by computing the integrity risk of each event hypothesis with double integral. The most difficulty in the implementation is to determine the worst HPE distribution center and the worst noncentrality parameter for each fault event hypothesis. By transforming the HPE into a new space in which the HPE has a unit covariance, the double integral has special characteristics and an upper bound for the worst HPE distribution center caused by both faults and nominal biases can be accordingly derived. Directly searching the worst noncentrality parameter along with the double integral for each fault event hypothesis is very computationally intensive. By replacing the elliptical double integral region with multiple small rectangles in the new space, the double integral can be conservatively computed using error function and the corresponding worst noncentrality parameter can hence be efficiently searched. The experiment shows that the proposed algorithm can significantly improve the HPL tightness compared to SS-ARAIM.

Appendix

Appendix A: Integral of two-dimensional normal distribution with distribution center changing along a line

The integral of the two-dimensional normal distribution $[x, y]^T \sim N\left([\mu_x, \mu_y]^T, \mathrm{diag}(\sigma_x, \sigma_y)\right)$ with an ellipse integral

region $\frac{x^2}{l_x^2}+\frac{y^2}{l_y^2}=1\ (0<l_x,0<l_y)$ can be expressed as follows:

$$P\left(\mu_x,\mu_y\right)=\int_{-l_y}^{l_y}\mathrm{d}y\int_{-l_x\sqrt{1-\frac{y^2}{l_y^2}}}^{l_x\sqrt{1-\frac{y^2}{l_y^2}}}\frac{1}{2\pi\sigma_x\sigma_y}e^{-\frac{1}{2}\left[\left(\frac{x-\mu_x}{\sigma_x}\right)^2+\left(\frac{y-\mu_y}{\sigma_y}\right)^2\right]}\mathrm{d}x \tag{59}$$

$P\left(\mu_x,\mu_y\right)$ is symmetric about the x-axis and the y-axis. Here, we only study the case in which the distribution center is in the first quadrant. The obtained results can be easily generalized to the entire xy plane. For any certain y, we have

$$\begin{aligned}&\frac{\mathrm{d}}{\mathrm{d}\mu_x}\left(\int_{-l_x\sqrt{1-\frac{y^2}{l_y^2}}}^{l_x\sqrt{1-\frac{y^2}{l_y^2}}}\frac{1}{\sqrt{2\pi}\sigma_x}e^{-\frac{1}{2}\left(\frac{x-\mu_x}{\sigma_x}\right)^2}\mathrm{d}x\right)\\&=\frac{1}{\sqrt{2\pi}\sigma_x}e^{-\frac{1}{2\sigma_x^2}\left(l_x\sqrt{1-\frac{y^2}{l_y^2}}+\mu_x\right)^2}-\frac{1}{\sqrt{2\pi}\sigma_x}e^{-\frac{1}{2\sigma_x^2}\left(l_x\sqrt{1-\frac{y^2}{l_y^2}}-\mu_x\right)^2}\\&=\begin{cases}>0 & ;\mu_x<0\\=0 & ;\mu_x=0\\<0 & ;\mu_x>0\end{cases}\end{aligned} \tag{60}$$

Hence, for any $\mu_x^a\ge\mu_x^b\ge 0$, we have

$$\begin{aligned}&P(\mu_x^a,\mu_y)-P(\mu_x^b,\mu_y)\\&=\int_{-l_y}^{l_y}\mathrm{d}y\int_{-l_x\sqrt{1-\frac{y^2}{l_y^2}}}^{l_x\sqrt{1-\frac{y^2}{l_y^2}}}\frac{1}{2\pi\sigma_x\sigma_y}e^{-\frac{1}{2}\left[\left(\frac{x-\mu_x^a}{\sigma_x}\right)^2+\left(\frac{y-\mu_y}{\sigma_y}\right)^2\right]}\mathrm{d}x\\&\quad-\int_{-l_y}^{l_y}\mathrm{d}y\int_{-l_x\sqrt{1-\frac{y^2}{l_y^2}}}^{l_x\sqrt{1-\frac{y^2}{l_y^2}}}\frac{1}{2\pi\sigma_x\sigma_y}e^{-\frac{1}{2}\left[\left(\frac{x-\mu_x^b}{\sigma_x}\right)^2+\left(\frac{y-\mu_y}{\sigma_y}\right)^2\right]}\mathrm{d}x\\&=\int_{-l_y}^{l_y}\frac{1}{\sqrt{2\pi}\sigma_y}e^{-\frac{1}{2}\left(\frac{y-\mu_y}{\sigma_y}\right)^2}\mathrm{d}y\\&\quad\times\int_{-l_x\sqrt{1-\frac{y^2}{l_y^2}}}^{l_x\sqrt{1-\frac{y^2}{l_y^2}}}\left(\frac{1}{\sqrt{2\pi}\sigma_x}e^{-\frac{1}{2}\left(\frac{x-\mu_x^a}{\sigma_x}\right)^2}-\frac{1}{\sqrt{2\pi}\sigma_x}e^{-\frac{1}{2}\left(\frac{x-\mu_x^b}{\sigma_x}\right)^2}\right)\mathrm{d}x\\&\le 0\end{aligned} \tag{61}$$

Equation (61) indicates that $P\left(\mu_x,\mu_y\right)$ has a greater value when the HPE distribution center is closer to the y-axis. Similarly, for any $\mu_y^a\ge\mu_y^b\ge 0$, we have

$$\begin{aligned}&P\left(\mu_x,\mu_y^a\right)-P\left(\mu_x,\mu_y^b\right)\\&=\int_{-l_y}^{l_y}\mathrm{d}y\int_{-l_x\sqrt{1-\frac{y^2}{l_y^2}}}^{l_x\sqrt{1-\frac{y^2}{l_y^2}}}\frac{1}{2\pi\sigma_x\sigma_y}e^{-\frac{1}{2}\left[\left(\frac{x-\mu_x}{\sigma_x}\right)^2+\left(\frac{y-\mu_y^a}{\sigma_y}\right)^2\right]}\mathrm{d}x\\&\quad-\int_{-l_y}^{l_y}\mathrm{d}y\int_{-l_x\sqrt{1-\frac{y^2}{l_y^2}}}^{l_x\sqrt{1-\frac{y^2}{l_y^2}}}\frac{1}{2\pi\sigma_x\sigma_y}e^{-\frac{1}{2}\left[\left(\frac{x-\mu_x}{\sigma_x}\right)^2+\left(\frac{y-\mu_y^b}{\sigma_y}\right)^2\right]}\mathrm{d}x\\&\le 0\end{aligned} \tag{62}$$

When the integral region is a rectangle $-l_x\le x\le l_x,-l_y\le y<l_y$, we have

$$\begin{aligned}&\frac{\mathrm{d}}{\mathrm{d}\mu_x}\left(\int_{-l_x}^{l_x}\frac{1}{\sqrt{2\pi}\sigma_x}e^{-\frac{1}{2}\left(\frac{x-\mu_x}{\sigma_x}\right)^2}\mathrm{d}x\right)\\&=\frac{1}{\sqrt{2\pi}\sigma_x}e^{-\frac{1}{2\sigma_x^2}(l_x+\mu_x)^2}-\frac{1}{\sqrt{2\pi}\sigma_x}e^{-\frac{1}{2\sigma_x^2}(l_x-\mu_x)^2}\\&=\begin{cases}>0; & \mu_x<0\\=0 & \mu_x=0\\<0 & \mu_x>0\end{cases}\end{aligned} \tag{63}$$

Hence, the integral of the two-dimensional normal distribution $[x,y]^T$ with the rectangle integral region has the similar properties as the integral with the ellipse integral region.

Appendix B: Integral of two-dimensional normal distribution with distribution center changing along a circular arc

The integral of the two-dimensional normal distribution $[x,y]^T\sim N\left([\mu_x,\mu_y]^T,\mathrm{diag}(\sigma_x,\sigma_y)\right)$, $\mu_x^2+\mu_y^2=\ell^2$, $\sigma_x=\sigma_y=\sigma$ with an integral region $\frac{x^2}{l_x^2}+\frac{y^2}{l_y^2}=1\,(0<l_x\le l_y)$ can be expressed as follows:

$$
\begin{aligned}
&P\left(\mu_x,\mu_y\right)\\
&=\int_{-l_y}^{l_y}\mathrm{d}y\int_{-l_x\sqrt{1-\frac{y^2}{l_y^2}}}^{l_x\sqrt{1-\frac{y^2}{l_y^2}}}\frac{1}{2\pi\sigma^2}e^{-\frac{1}{2}\left[\left(\frac{x-\mu_x}{\sigma}\right)^2+\left(\frac{y-\mu_y}{\sigma}\right)^2\right]}\mathrm{d}x\\
&=P(\ell,\varphi)\\
&=\int_{-l_y}^{l_y}\mathrm{d}y\int_{-l_x\sqrt{1-\frac{y^2}{l_y^2}}}^{l_x\sqrt{1-\frac{y^2}{l_y^2}}}\frac{1}{2\pi\sigma^2}e^{-\frac{1}{2}\left[\left(\frac{x-\ell\cos(\varphi)}{\sigma}\right)^2+\left(\frac{y-\ell\sin(\varphi)}{\sigma}\right)^2\right]}\mathrm{d}x
\end{aligned}
\tag{64}
$$

where $\mu_x=\ell\cos(\varphi)$, $\mu_y=\ell\sin(\varphi)$. Consider that $P\left(\mu_x,\mu_y\right)$ is symmetric about the x-axis and the y-axis. Here, we also only discuss the situation in which the distribution center is in the first quadrant with $\mu_x\geq 0,\mu_y\geq 0$ and $0\leq\varphi\leq\pi/2$. Then, we have

$$
\begin{aligned}
\frac{\mathrm{d}}{\mathrm{d}\varphi}P(\ell,\varphi)&=\int_{-l_y}^{l_y}\mathrm{d}y\int_{-l_x\sqrt{1-\frac{y^2}{l_y^2}}}^{l_x\sqrt{1-\frac{y^2}{l_y^2}}}\left(\begin{array}{l}\frac{1}{\sigma^2}(y\ell\cos(\varphi)-x\ell\sin(\varphi))\\ \times\frac{1}{2\pi\sigma^2}e^{-\frac{1}{2}\left[\left(\frac{x-\ell\cos(\varphi)}{\sigma}\right)^2+\left(\frac{y-\ell\sin(\varphi)}{\sigma}\right)^2\right]}\end{array}\right)\mathrm{d}x\\
&=\int_{-l_y}^{l_y}\mathrm{d}y\int_{-l_x\sqrt{1-\frac{y^2}{l_y^2}}}^{l_x\sqrt{1-\frac{y^2}{l_y^2}}}\frac{1}{2\pi\sigma^4}\left(y\mu_x-x\mu_y\right)e^{-\frac{1}{2}\left[\left(\frac{x-\mu_x}{\sigma}\right)^2+\left(\frac{y-\mu_y}{\sigma}\right)^2\right]}\mathrm{d}x
\end{aligned}
\tag{65}
$$

The integral region is split by a line defined as follows:

$$
y\mu_x-x\mu_y=0\Rightarrow y=\frac{\mu_y}{\mu_x}x \tag{66}
$$

As shown in Fig. 10, the integral region is symmetric about the origin and can be divided into four smaller regions,

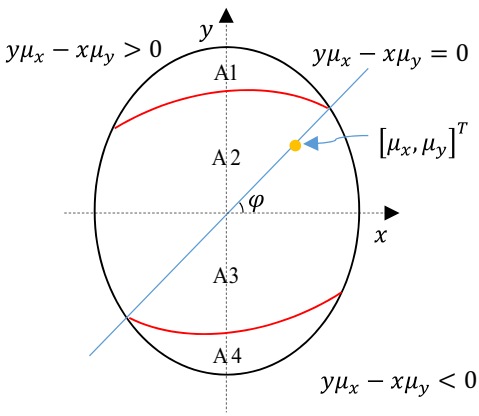

Fig. 10 Integral region division

respectively, labeled as A1, A2, A3 and A4. For $P\left(\mu_x,\mu_y\right)$ and $P(r,\varphi)$, regions A2 and A3 are symmetric about the line defined by (66), and region A4 is farther from the distribution center $\left(\mu_x,\mu_y\right)^T$ than region A1. Hence,

$$
\begin{aligned}
\frac{\mathrm{d}}{\mathrm{d}\varphi}P(\ell,\varphi)&=\int_{-l_y}^{l_y}\mathrm{d}y\int_{-l_x\sqrt{1-\frac{y^2}{l_y^2}}}^{l_x\sqrt{1-\frac{y^2}{l_y^2}}}\frac{1}{2\pi\sigma^4}\left(y\mu_x-x\mu_y\right)e^{-\frac{1}{2}\left[\left(\frac{x-\mu_x}{\sigma}\right)^2+\left(\frac{y-\mu_y}{\sigma}\right)^2\right]}\mathrm{d}x\\
&\geq 0
\end{aligned}
\tag{67}
$$

Equation (67) indicates that $P\left(\mu_x,\mu_y\right)$ is monotonically increasing along the circular arc $\varphi:0\rightarrow\pi/2$.

References

Benaskeur AR (2002) Consistent fusion of correlated data sources. In: Proceedings of the IEEE 2002 28th annual conference of the industrial electronics society. IECON 02. Sevilla, Spain, pp 2652–2656

Bhattacharyya S, Gebre-Egziabher D (2014) Integrity monitoring with vector GNSS receivers. IEEE Trans Aerosp Electron Syst 50(4):2779–2793

Bhattacharyya S, Gebre-Egziabher D (2015) Kalman filter–based RAIM for GNSS receivers. IEEE Trans Aerosp Electron Syst 51(3):2444–2459

Blanch J, Walter T (2020a) Fast protection levels for fault detection with an application to advanced RAIM. IEEE Trans Aerosp Electron Syst 57(1):55–65

Blanch J, Walter T (2020b) Stress testing advanced RAIM airborne algorithms. In: Proceedings of the ION ITM 2020, Institute of Navigation, San Diego, California, USA, pp 421–439

Blanch J, Walker T, Enge P, Lee YC, Pervan B, Rippl M, Spletter A, Kropp V (2015) Baseline advanced RAIM user algorithm and possible improvements. IEEE Trans Aerosp Electron Syst 51(1):713–732

Brenner M (1996) Integrated GPS/inertial fault detection availability. Navigation 43(2):111–130

Brown RG, Chin GY (1998) GPS RAIM: calculation of the threshold and protection radius using chi-square methods-a geometric approach. The Institute of Navigation's Special Monograph Series on GPS V, pp 155–178

Diesel J, Luu S (1995) GPS/IRS AIME: calculation of thresholds and protection radius using chi-square methods. In: Proceedings of the ION GPS 1995, Institute of Navigation, Palm Springs, California, USA, September 12–15, pp 1959–1964

Feng SJ, Ochieng WY, Walsh D, Ioannides R (2006) A measurement domain receiver autonomous integrity monitoring algorithm. GPS Solut 10(2):85–96

International Civil Aviation Organization (ICAO) (2006) Aeronautical telecommunications. Annex 10 to the convention on international civil aviation. Volume I radio navigation aids

Jiang Y, Wang J (2014) A new approach to calculate the vertical protection level in A-RAIM. J Navig 67(4):711–725

Jiang Y, Wang J (2016) A new approach to calculate the horizontal protection level. J Navig 69(1):57–74

Joerger M, Pervan B (2013) Kalman filter-based integrity monitoring against sensor faults. J Guid Control Dyn 36(2):349–361

Joerger M, Pervan B (2016) Fault detection and exclusion using solution separation and chi-squared ARAIM. IEEE Trans Aerosp Electron Syst 52(2):726–742
Liu BY, Zhan XQ, Zheng HZhu (2017) Multisensor parallel largest ellipsoid distributed data fusion with unknown cross-covariances. Sensors 17(7):1526
Milner CD, Ochieng WY (2010) A fast and efficient integrity computation for non-precision approach performance assessment. GPS Solut 14(2):193–205
Milner CD, Ochieng WY (2011) Weighted RAIM for APV: the ideal protection level. J Navig 64(1):61–73
Ober PB (1998) RAIM performance: how algorithms differ. In: Proceedings of the ION GPS 1998, Institute of Navigation, Nashville, Tennessee, USA, September 15–18, pp 2021–2030
Parkinson BW, Axelrad P (1988) Autonomous GPS integrity monitoring using the pseudorange residual. Navigation 35(2):255–274
Pervan B (1996) Navigation integrity for aircraft precision landing using the global positioning system. Dissertation, Stanford University
Sturza MA (1988) Navigation system integrity monitoring using redundant measurements. Navigation 35(4):483–501
Tanıl Ç, Khanafseh S, Joerger M, Pervan B (2018) An INS monitor to detect GNSS spoofers capable of tracking vehicle position. IEEE Trans Aerosp Electron Syst 54(1):131–143
Walter T, Enge P (1995) Weighted RAIM for precision approach. In: Proceedings of the ION GPS 1995, Institute of Navigation, Palm Springs, California, USA, September 12–15, pp 1995–2004
Wang SZ, Zhan XQ, Zhai YW, Liu BY (2020) Fault detection and exclusion for tightly coupled GNSS/INS system considering fault in state prediction. Sensors 20(3):590

Baoyu Liu is a postdoc at the University of Calgary. His research interests include GNSS/INS integrated navigation, GNSS integrity monitoring, data fusion algorithms and software-defined receiver.

Yang Gao is a professor in the Department of Geomatics Engineering at the University of Calgary. His expertise includes theoretical aspects and practical applications of satellite-based positioning and navigation systems, high precision GNSS positioning, and multi-sensor integrated navigation systems.

Yuting Gao is a Ph.D. candidate at the University of Calgary. Her current research focuses on the integrity monitoring of GNSS precise positioning, low-cost GNSS receivers and multi-sensor integrated navigation systems.

Shizhuang Wang is a Ph.D. candidate at Shanghai Jiao Tong University. His research interests focus on multi-sensor integration, fault detection and exclusion, and integrity monitoring.